Double Fano resonances in a composite metamaterial possessing tripod plasmonic resonances

Article *in* Journal of Optics · September 2013

DOI: 10.1088/2040-8978/17/2/025103 · Source: arXiv

Double Fano resonances in a composite metamaterial possessing tripod plasmonic resonances

Y.U. Lee,[1] E.Y. Choi,[1] E.S. Kim,[1] J.H. Woo,[1] B. Kang,[1] J. Kim,[1] Byung Cheol Park,[2] T.Y. Hong,[2] Jae Hoon Kim,[2] and J.W. Wu[1,*]

[1] *Department of Physics and Quantum Metamaterials Research Center, Ewha Womans University, Seoul 120-750, Korea*

[2] *Department of Physics, Yonsei University, Seoul 120-749, Korea*

[*] *jwwu@ewha.ac.kr*

Abstract: By embedding four-rod resonators inside double-split ring resonators superlattice, a planar composite metamaterial possessing tripod plasmonic resonances is fabricated. Double Fano resonances are observed where a common subradiant driven oscillator is coupled with two superradiant oscillators. As a classical analogue of four-level tripod atomic system, the transmission spectrum of the composite metamaterial exhibits a double Fano-based coherent effect. Transfer of absorbed power between two superradiant oscillators is controlled by manipulating two coupling strengths conjugated through the polarization angle of a normally incident electromagnetic wave.

OCIS codes: (160.3918) Metamaterials;(300.6495) Spectroscopy, Terahertz.

References and links

1. N. Verellen, Y. Sonnefraud, H. Sobhani, F. Hao, V. V. Moshchalkov, P. V. Dorpe, P. Nordlander, and S. A. Maier, "Fano resonances in individual coherent plasmonic nanocavities," Nano Lett. **9**, 1663–1667 (2009).
2. A. E. Miroshnichenko, S. Flach, and Y. S. Kivshar, "Fano resonances in nanoscale structures," Rev. Mod. Phys. **82**, 2257–2298 (2010).
3. B. Luk'yanchuk, N. I. Zheludev, S. A. Maier, N. J. Halas, P. Nordlander, H. Giessen, and C. T. Chong, "The fano resonance in plasmonic nanostructures and metamaterials," Nat. Mater. **9**, 707–715 (2010).
4. S. Zhang, D. A. Genov, Y. Wang, M. Liu, and X. Zhang, "Plasmon-induced transparency in metamaterials," Phys. Rev. Lett. **101**, 047401 (2008).
5. N. Liu, L. Langguth, T. Weiss, J. Kastel, M. Fleischhauer, T. Pfau, and H. Giessen, "Plasmonic analogue of electromagnetically induced transparency at the drude damping limit," Nat. Mater. **8**, 758–762 (2009).
6. N. Liu, T. Weiss, M. Mesch, L. Langguth, U. Eigenthaler, M. Hirscher, C. Sonnichsen, and H. Giessen, "Planar metamaterial analogue of electromagnetically induced transparency for plasmonic sensing," Nano Lett. **10**, 1103–1107 (2010).
7. X. Liu, J. Gu, R. Singh, Y. Ma, J. Zhu, Z. Tian, M. He, J. Han, and W. Zhang, "Electromagnetically induced transparency in terahertz plasmonic metamaterials via dual excitation pathways of the dark mode," Appl. Phys. Lett. **100**, 131101–131101 (2012).
8. J. Wang, C. Fan, J. He, P. Ding, E. Liang, and Q. Xue, "Double fano resonances due to interplay of electric and magnetic plasmon modes in planar plasmonic structure with high sensing sensitivity," Opt. Express **21**, 2236–2244 (2013).
9. S.-D. Liu, Z. Yang, R.-P. Liu, and X.-Y. Li, "Multiple fano resonances in plasmonic heptamer clusters composed of split nanorings," ACS nano **6**, 6260–6271 (2012).
10. S.-D. Liu, M.-J. Zhang, W.-J. Wang, and Y.-C. Wang, "Tuning multiple fano resonances in plasmonic pentamer clusters," Appl. Phys. Lett. **102**, 133105–133105 (2013).

11. N. Liu, M. Hentschel, T. Weiss, A. P. Alivisatos, and H. Giessen, "Three-dimensional plasmon rulers," Science **332**, 1407–1410 (2011).
12. T. J. Davis, M. Hentschel, N. Liu, and H. Giessen, "Analytical model of the three-dimensional plasmonic ruler," ACS nano **6**, 1291–1298 (2012).
13. A. Artar, A. A. Yanik, and H. Altug, "Multispectral plasmon induced transparency in coupled meta-atoms," Nano Lett. **11**, 1685–1689 (2011).
14. S. Rebić, D. Vitali, C. Ottaviani, P. Tombesi, M. Artoni, F. Cataliotti, and R. Corbalan, "Polarization phase gate with a tripod atomic system," Phys. Rev. A **70**, 032317 (2004).
15. S. Li, X. Yang, X. Cao, C. Zhang, C. Xie, and H. Wang, "Enhanced cross-phase modulation based on a double electromagnetically induced transparency in a four-level tripod atomic system," Phys. Rev. Lett. **101**, 073602 (2008).
16. A. MacRae, G. Campbell, and A. Lvovsky, "Matched slow pulses using double electromagnetically induced transparency," Opt. Lett. **33**, 2659–2661 (2008).
17. Y. He and K.-D. Zhu, "Fano correlation effect of optical response due to plasmon–exciton–plasmon interaction in an artificial hybrid molecule system," J. Opt. Soc. Am. B **30**, 868–873 (2013).
18. Z. Bai, C. Hang, and G. Huang, "Classical analogs of double electromagnetically induced transparency," Opt. Commun. **291**, 253–258 (2013).
19. U. Fano, "Effects of configuration interaction on intensities and phase shifts," Phys. Rev. **124**, 1866–1878 (1961).
20. B. Gallinet and O. J. F. Martin, "Ab initio theory of fano resonances in plasmonic nanostructures and metamaterials," Phys. Rev. B **83**, 235427 (2011).
21. B. Gallinet and O. J. F. Martin, "Relation between near–field and far–field properties of plasmonic fano resonances," Opt. Express **19**, 22167–22175 (2011).
22. C. G. Alzar, M. Martinez, and P. Nussenzveig, "Classical analog of electromagnetically induced transparency," Am. J. Phys. **70**, 37 (2002).
23. B. Gallinet, T. Siegfried, H. Sigg, P. Nordlander, O. Martin *et al.*, "Plasmonic radiance: probing structure at the angstrom scale with visible light." Nano Lett. **13**, 497–503 (2013).
24. F. López-Tejeira, R. Paniagua-Domínguez, R. Rodríguez-Oliveros, and J. Sánchez-Gil, "Fano-like interference of plasmon resonances at a single rod-shaped nanoantenna," New J. Phys. **14**, 023035 (2012).
25. F. Hao, Y. Sonnefraud, P. V. Dorpe, S. A. Maier, N. J. Halas, and P. Nordlander, "Symmetry breaking in plasmonic nanocavities: subradiant lspr sensing and a tunable fano resonance," Nano Lett. **8**, 3983–3988 (2008).
26. F. Hao, E. M. Larsson, T. A. Ali, D. S. Sutherland, and P. Nordlander, "Shedding light on dark plasmons in gold nanorings," Chem. Phys. Lett. **458**, 262–266 (2008).
27. M. Frimmer, T. Coenen, and A. F. Koenderink, "Signature of a fano resonance in a plasmonic metamolecule's local density of optical states," Phys. Rev. Lett. **108**, 077404 (2012).
28. B. Gallinet and O. J. Martin, "Influence of electromagnetic interactions on the line shape of plasmonic fano resonances," ACS nano **5**, 8999–9008 (2011).
29. A. Lovera, B. Gallinet, P. Nordlander, and O. J. Martin, "Mechanisms of fano resonances in coupled plasmonic systems," ACS nano **6** 4527–4536 (2013).
30. B. Kang, J. Woo, E. Choi, H.-H. Lee, E. Kim, J. Kim, T.-J. Hwang, Y.-S. Park, D. Kim, and J. Wu, "Optical switching of near infrared light transmission in metamaterial-liquid crystal cell structure," Opt. Express **18**, 16492–16498 (2010).
31. J. Woo, E. Kim, E. Choi, B. Kang, H.-H. Lee, J. Kim, Y. Lee, T. Y. Hong, J. H. Kim, and J. Wu, "Cryogenic temperature measurement of thz meta-resonance in symmetric metamaterial superlattice," Opt. Express **19**, 4384–4392 (2011).
32. "See http://www.teraview.com," .
33. Y. S. Joe, A. M. Satanin, and C. S. Kim, "Classical analogy of fano resonances," Phys. Scripta **74**, 259–266 (2006).
34. J. Gu, R. Singh, X. Liu, X. Zhang, Y. Ma, S. Zhang, S. A. Maier, Z. Tian, A. K. Azad, H.-T. Chen *et al.*, "Active control of electromagnetically induced transparency analogue in terahertz metamaterials," Nat. Commun. **3**, 1151 (2012).
35. X. Shen and T. J. Cui, "Photoexcited broadband redshift switch and strength modulation of terahertz metamaterial absorber," J. Optics **14**, 114012 (2012).
36. X. jun He, J. min Wang, X. hua Tian, J. xing Jiang, and Z. xin Geng, "Dual-spectral plasmon electromagnetically induced transparency in planar metamaterials based on bright-dark coupling," Opt. Commun. **291**, 371 – 375 (2013).
37. A. Bitzer, A. Ortner, H. Merbold, T. Feurer, and M. Walther, "Terahertz near-field microscopy of complementary planar metamaterials: Babinet's principle," Opt. Express **19**, 2537–2545 (2011).
38. A. Artar, A. A. Yanik, and H. Altug, "Directional double fano resonances in plasmonic hetero-oligomers," Nano Lett. **11**, 3694–3700 (2011).

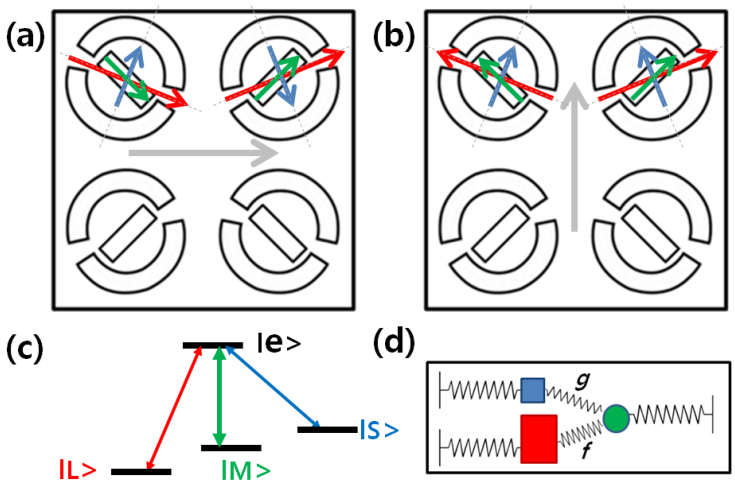

Fig. 1. Schematics of a composite metamaterial is shown with the dipoles in four-rod resonator and double-split ring resonator superlattice for a normally incident wave with (a) horizontal and (b) vertical polarization. (c) Four-level tripod is shown. (d) Classical model of one subradiant oscillator coupled with two superradiant oscillators is shown with coupling strength f and g.

1. Introduction

Control of Fano resonance has been a focus of research in artificially structured nano-sized materials including quantum dots, nano-wires, photonic-crystal slabs, plasmonic nanostructures, as well as metamaterials [1–3]. Metamaterials can be designed to possess a broad bright mode and a non-resonant dark mode, which couples each other to exhibit a destructive interference effect such as classical analogue of electromagnetically induced transparency (EIT) phenomenon, corresponding to a Fano resonance with the asymmetry parameter equal to zero [4–6].

As a further development to engineer metamaterials having a higher sensitivity as well as a broad spectral response for sensor application, multiple Fano resonances are investigated in plasmonic metamaterials. Multiple Fano resonances can be achieved in two different schemes. The first scheme is to employ one bright mode and two or more dark modes. Examples are abundant where a bright dipole couples with two dark dipoles or quadrupoles: one bright dipole resonator and a pair of split ring resonators (SRRs) as the dark elements [7], double symmetrical U-shaped SRRs with a nanorod between the two SRRs [8], plasmonic clusters of heptamer [9] and pentamer [10], and 3D metamaterials [11–13].

The second scheme is to employ one dark mode and two or more bright modes, which already has been utilized in a four-level tripod atomic system to achieve quantum coherent effects such as polarization photon gate [14], enhanced cross-phase modulation [15], and two slow-pulse matching [16]. In the four-level tripod atomic system, two different low-lying energy levels $|L>$ and $|S>$, bright states, are coupled to a common excited state $|e>$ by weak probe and trigger lasers, while the third low-lying energy level $|M>$, dark state, is coupled to the excited state $|e>$ by a strong pumping laser to provide pathways to both probe and trigger lasers necessary for double EITs. While a quantum coherence of $|L>$ and $|S>$ is maintained, double EIT-based coherent effects are observed. As a classical analogue, a theoretical analysis of Fano correlation effect is reported for a plasmon-exciton-plasmon interaction in an artificial hybrid molecular system, one quantum dot placed in the gap of two identical metal nanoparticles

[17]. A classical model has already been introduced, where two bright oscillators with different resonance frequencies are coupled to one dark oscillator [18].

In this work, we experimentally demonstrate a classical analogue of double Fano resonances in a planar composite metamaterial possessing tripod plasmonic resonances, where a common subradiant dipole corresponding to a dark mode is coupled with two superradient dipoles corresponding to two bright modes. The composite metamaterial is structured such that four-rod resonators (FRR) are embedded inside double-split ring resonators (DSRR) superlattice. See Fig. 1. Two dipole resonances of DSRR are superradiant modes corresponding to the excitations of $|L>\rightarrow|e>$ and $|S>\rightarrow|e>$, and one dipole resonance of FRR is subradiant mode corresponding to the excitation of $|M>\rightarrow|e>$. Proximity of the inner diameter of DSRR and the rod-length of FRR permits near-field coherent couplings, and the composite metamaterial is a tripod metamaterial system possessing two superradiant dipole resonances of DSRR coupled coherently with one common subradiant dipole resonance of FRR in near-field, similar to a tripod atomic system with four atomic levels coupled coherently by coherent optical fields.

Important finding is that double Fano resonances in the composite metamaterial are correlated owing to the conjugation of two coupling strengths f and g, showing up as a transfer of absorbed power from one superradiant dipole to the other superradient dipole in DSRR. The dipole resonance in FRR is polarization-independent, while two dipole resonances in DSRR are polarization-dependent, which allows for a control of the transfer of absorbed power by manipulating the polarization angle of a normally incident electromagnetic wave.

In Sec.2, a general feature of plasmonic Fano resonance is examined where both superradiant and subradiant oscillators are externally driven. An analysis based on two coupled oscillators model leads to that a general Fano resonance formula of plasmonic structure is kept the same with a modification in the asymmetry parameter q. In Sec.3, we introduce a planar composite metamaterial possessing tripod plasmonic resonances, and a THz transmission spectrum of the fabricated sample is presented along with the finite-difference-time-domain (FDTD) simulated spectrum. In Sec.4, the double Fano resonances are analyzed analytically by a set of coupled equations of motion of two superradiant oscillators and one subradiant oscillators to identify coherent processes of the energy transfer between two superradiant oscillators. In particular, the phase evolutions of superradiant and subradiant oscillators are closely examined. In Sec.5, the multipolar nature of near-field coherent interaction is examined by the electric field distribution obtained from finite-difference-time-domain theoretical simulation. Sec.6 summarizes the major findings with conclusion.

2. Fano resonance in two coupled superradiant and subradiant oscillators simultaneously driven

Originally Fano resonance is introduced by examining an asymmetric peak in an excitation spectra observed near autoionization discrete energy level overlapping with continuum energy level of helium [19]. While the discrete state (dark mode) is not directly excited, a rapid π phase change takes place near the discrete resonance in the presence of a slowly varying-phase background continuum (bright mode). The constructive and destructive dispersive interferences give rise to an asymmetric line shape in the continuum spectrum, and the sequence of spectral positions of two interferences depends on whether the discrete resonance falls on the red or blue side of the background continuum resonance. The asymmetric Fano line shape is characterized by 3 parameters, the resonance shift Δ, the resonance width Γ, and the asymmetry parameter q.

Differently from the dark mode in atomic spectroscopy, in metallic plasmonic structures there exits an intrinsic loss γ_i in dark mode, and Gallinet *et al.* [20] obtained a general formula of Fano-like asymmetric line shape by introducing a modulation damping parameter b, a measure of the decrease in Fano resonance contrast [21]. It is also shown that a classical two coupled

oscillators model [22] with a lossy dark oscillator provides the same general formula when the complex amplitude is expanded near the dark resonance [23].

On the other hand, a far-field Fano-like asymmetric line shape is observed in plasmonic structures without resorting to a plasmonic dark mode. The occurrence of a Fano-like interference in a single nano-rod plasmonic structures is attributed to a spatial overlap of two non-orthogonal adjacent plasmonic modes [24], and in a nonconcentric ring/disk cavity plasmonic structure Fano line shape still persists when dark multipolar resonances are optically excited by a retardation effect at a non-normal incidence angle [25, 26]. Furthermore, in a heptamer plasmonic nanostructure composed of one center disc with surrounding hexamer ring, an examination of local density of optical states by a selective e-beam excitation of center and ring showed that a far-field interference between the dressed superradiant (large dipole moment, strongly driven) and subradiant (small dipole moment, weakly driven) eigenmodes fully describes Fano resonance [27]. In fact asymmetric Fano line shape observed in a variety of plasmonic structures are fitted to the general Fano formula with an excellent agreement [28]. These studies lead to the notion that in plasmonic structures an interference between superradiant and subradient eigenmodes overlapping both spectrally and spatially gives rise to an asymmetric Fano line shape resonance [24, 29].

Now we raise the question whether the asymmetric Fano line shape is retained when both superradiant and subradiant oscillators are driven simultaneously in the presence of a coherent coupling. We examine how the broad Lorentzian spectrum of a superradiant oscillator is modified when coupled with a driven subradiant narrow oscillator by adopting a simple mechanical two coupled oscillators model. Two coupled oscillators are described by a set of equations of motion.

$$\frac{d^2x_b}{dt^2} + \gamma_b \frac{dx_b}{dt} + \omega_b^2 x_b + g x_d = f_1 e^{i\omega t} \tag{1}$$

$$\frac{d^2x_d}{dt^2} + \gamma_d \frac{dx_d}{dt} + \omega_d^2 x_d + g x_b = f_2 e^{i\omega t} \tag{2}$$

The narrow spectrum of subradiant oscillator d is located within the broad spectrum of superradiant oscillator b. Putting $x_b = c_b e^{i\omega t}$, we obtain the amplitude c_b of the superradiant oscillator b near the resonance ω_d of narrow subradiant oscillator d.

$$\begin{aligned} c_b(\omega) &= \frac{(\omega_d^2 + i\gamma_d\omega - \omega^2)f_1 - g f_2}{L_\omega(\omega_d^2 + i\gamma_d\omega - \omega^2) - g^2} \\ &= \frac{f_1}{L_\omega} \cdot \frac{(\omega_d^2 + i\gamma_d\omega - \omega^2 - g\frac{f_2}{f_1})L_\omega}{L_\omega(\omega_d^2 + i\gamma_d\omega - \omega^2) - g^2} \\ &\approx \frac{f_1}{L_\omega} \cdot \frac{(\omega_d^2 + i\gamma_d\omega - \omega^2 - g\frac{f_2}{f_1})L_d}{L_d(\omega_d^2 + i\gamma_d\omega - \omega^2) - g^2} \end{aligned}$$

where $L_\omega \equiv \omega_b^2 + i\gamma_b\omega - \omega^2$ and $L_d = \omega_b^2 + i\gamma_b\omega_d - \omega_d^2$. An external driving f_2 of the subradiant oscillator contributes to the superradiant amplitude via a coupling g. Following the procedure in Ref. [23], the spectrum of superradiant oscillator has the following relation.

$$|c_b|^2 \approx \frac{f_1^2}{|L_\omega|^2} \cdot \frac{(\kappa + q_1)^2 + b}{\kappa^2 + 1}$$

where

$$q_1 = q + \frac{g}{\Gamma}\frac{f_2}{f_1}.$$

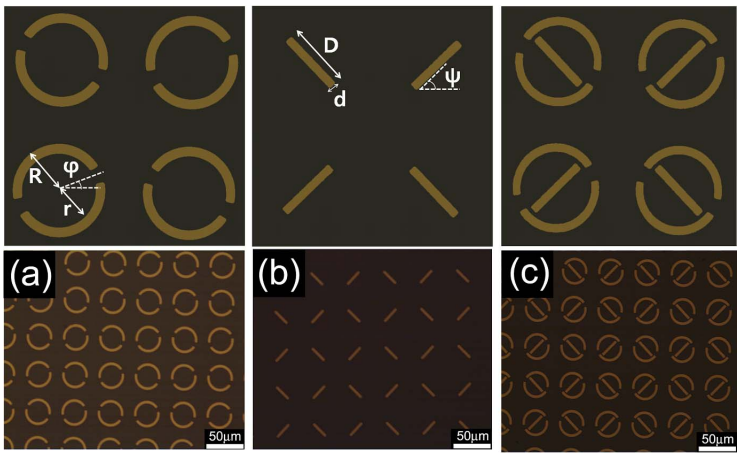

Fig. 2. Optical microscopy images and structural dimensions of (a) double-split ring resonator metamaterial, MM**1**, (b) four-rod resonator metamaterial, MM**2**, and (c) composite metamaterial, MM**3** are shown. R=18 μm, r=14 μm, φ= 22.5°, and D=26 μm, d=4 μm, ψ=45°.

The formula of asymmetric Fano resonance line shape reported in Ref. [23] is kept the same as a closed form with a modification in the asymmetry parameter from q to q_1.

We observe that a dark mode is not necessarily prerequisite for an asymmetric Fano resonance to take place in plasmonic structures. The dark mode is one example of non-driven narrow oscillators. The characteristic asymmetry feature of Fano resonance in plasmonic structures is retained even in the presence of an external driving of narrow oscillator as far as a dispersive coherent coupling between two oscillators ensures a π-phase shift in the broad superradiant oscillator near the narrow subradiant oscillator resonance.

3. Sample design & fabrication and terahertz spectra

3.1. Sample design & fabrication

DSRR exhibits two perpendicular dipolar resonances, a low-Q ω_L and a high-Q ω_H, which is equivalent to the notion that one DSRR accommodates two independent dipole oscillators with resonances at ω_L and ω_H [30]. In the superlattice array, DSRRs are arrayed in a square lattice such that the gap orientation is rotated by an angle $\varphi = \pm\frac{\pi}{8}$ alternately with respect to the horizontal direction (x-axis), which allows simultaneous excitations of both low-Q ω_L and high-Q ω_H resonances of DSRR upon incidence of a linearly polarized electromagnetic wave. The amount of relative excitations of ω_L and ω_H dipole oscillators depends on the angle between the polarization direction and the gap orientation of DSRR [31]. On the other hand, the FRR possesses one dipole resonance, ω_M, that is, FRR accommodates one dipole oscillator with resonance at ω_M.

The metamaterials are fabricated by standard photo-lithography and lift-off process of gold film with a micrometer resolution, which is prepared from e-beam evaporation of 10nm thick titanium adhesion layer and 200nm thick gold layers on 0.5mm thick p-doped Si wafer. We call DSRR metamaterial, FRR metamaterial, and the composite metamaterial as MM**1** , MM**2**, and MM**3**, respectively, and optical microscopy images are shown in Fig. 2 (a), (b), and (c), with structural dimensions. MM**1** is a superlattice array of DSRRs with the inner radius r=14 μm, the outer radius R=18 μm, the width of circle line 4μm, which are arranged with the gap

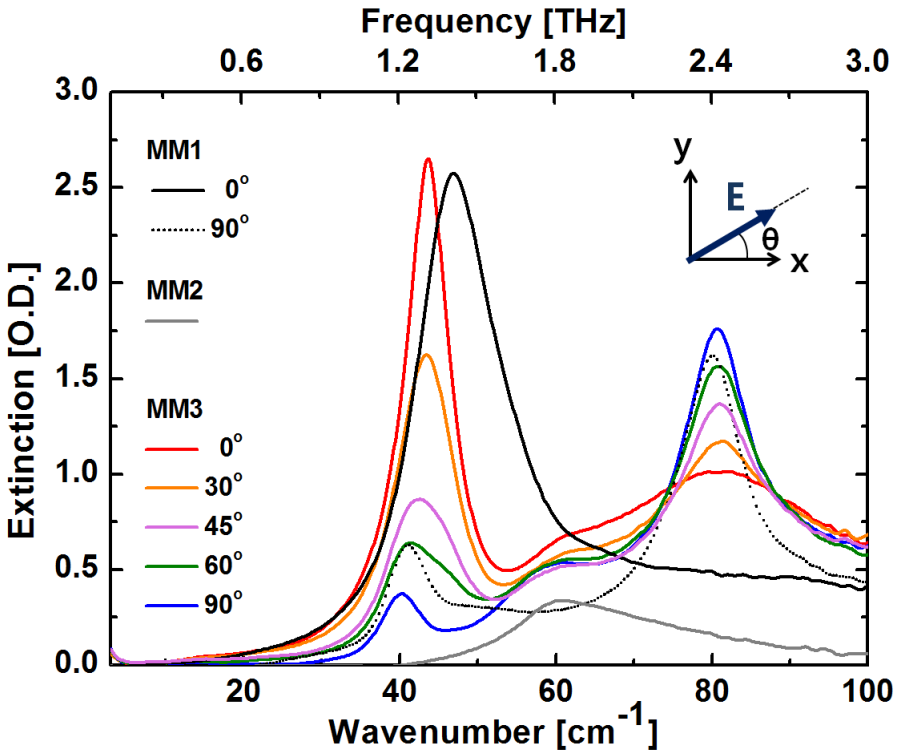

Fig. 3. Optical density plots of THz transmission spectrum of MM**3** for polarization angles of $\theta = 0°$, 30°, 45°, 60°, and 90° are shown. Black solid curve and black dashed curves correspond to transmission spectrum of MM**1** at polarization angles of $\theta = 0°$ and 90°, while gray solid curve correspond to transmission spectrum of MM**2**.

orientation $\varphi = \pm\frac{\pi}{8}$ and the lattice constant 50 μm. Previous study showed that MM**1** exhibits two polarization-dependent dipole resonances with different Q-values in the spectral range of 0.1-3.0 THz. MM**2** is an array of FRRs with $\psi = \frac{\pi}{4}$, D=26 μm, d=4 μm, and the lattice constant 50 μm. The relative orientation of rods, i.e., $\frac{\pi}{2}$, is set such that electromagnetic response of MM**2** is the same regardless of the polarization angle in an effective medium approximation. That is, MM**2** is isotropic with respect to the polarization direction. We note that the relative orientation of split-rings in DSRR and rods in FRR entails non-symmetric dipolar interactions between rod of FRR and split-ring of DSRR for the upper and lower arc split-rings in MM**3**.

3.2. Terahertz transmission spectrum measurement and FDTD simulation spectrum

Time-domain polarized terahertz transmission measurements are carried out by a Teraview TPS Spectra 3000 Spectrometer [32] with a resolution of 1.2 cm^{-1} at room temperature in vacuum. Sample size is 10×10 mm^2 and THz beam diameter is about 5mm. Fig. 3 shows the optical density plots of THz transmission spectrum of MM**3** at a series of polarization angles along with those of MM**1** at polarization angles of $\theta = 0°$ (x-axis) and 90° (y-axis) as well as MM**2**. Figure 4 shows optical density plots of simulated spectra at a series of polarization angles for (a) MM**1** and MM**2** (gray curve) and (b) MM**3** along with MM**1** at $\theta = 0°$ (black solid curve)

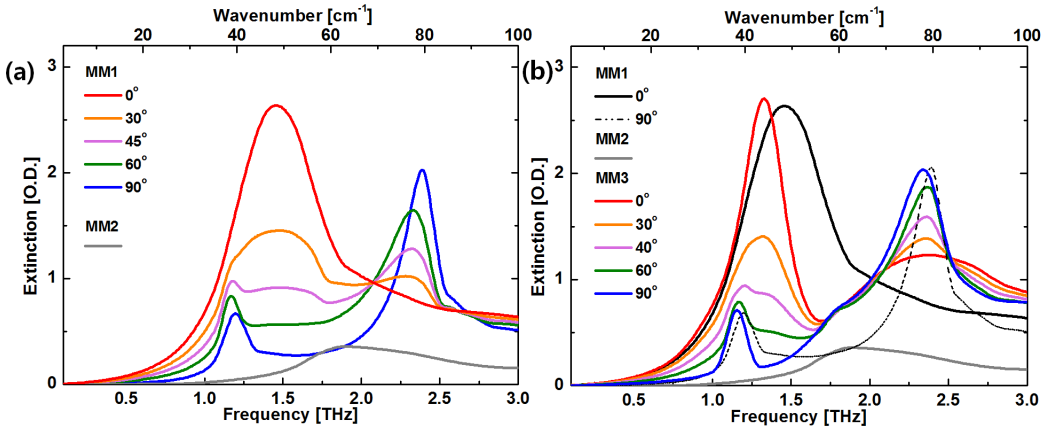

Fig. 4. Optical density plots of simulated spectra are shown at a series of polarization angles for (a) MM**1** and MM**2** (gray curve) and (b) MM**3** along with MM**1** at $\theta = 0^\circ$ (black solid curve) and $\theta = 90^\circ$ (black dotted curve)and MM**2** (gray curve).

and $\theta = 90^\circ$ (black dotted curve)and MM**2** (gray curve). Comparison of Fig. 3 and Fig. 4(b) shows that there is an excellent agreement between the measured and FDTD simulated spectra.

Let's note the characteristics of MM**1** and MM**2** spectra in Fig. 4(a). Resonances in MM**1** spectrum are polarization-dependent. For $\theta = 0^\circ$ one low-Q resonance with a large oscillator strength is excited at a low-frequency ω_L = 1.4THz and the other broad resonance with a small oscillator strength stretches with high-frequency ω_H ranging from 1.8THz to 3.0THz, and for $\theta = 90^\circ$ two resonances are excited, a high-Q resonance with a small oscillator strength at low-frequency ω_L = 1.2THz and a low-Q resonance with a large oscillator strength at high-frequency ω_H = 2.4THz, which is characteristic of superlattice structure of DSRRs as discussed in [31]. On the other hand, MM**2** possesses one low-Q resonance with the resonance frequency $\omega_M \approx$ 1.8THz, and the spectral shape and position are independent of the polarization angle θ.

Comparison of the linear absorption spectra of MM**1** and MM**2** shows two notable features. First, the total absorption cross section of MM**1** is much larger that that of MM**2**, showing that a direct coupling with the incident electric field is much stronger in MM**1** than MM**2**. Therefore, MM**3** is composed of strongly driven MM**1** and and weakly driven MM**2** oscillators interacting by a near-field coupling. Second, the entire spectrum of MM**2** is contained under the envelope of the spectrum of MM**1**, meaning that spectral width of MM**2** is considerably narrower than that of MM**1**. This leads to the correspondence of MM**1** and MM**2** to a broad superradiant oscillator and a narrow subradiant oscillator, respectively.

Next, we examine MM**3** spectrum qualitatively by paying attention to changes at the low-frequency and high-frequency peaks. At the low-frequency peaks, comparison of MM**1** spectrum in Fig. 4(a) and MM**3** spectrum in Fig. 4(b) shows that there occur dips on the blue side of the low-frequency peaks for all the polarization angle θ. On the other hand, at the high-frequency peaks, the most noteworthy change is that the extinction is enhanced almost two-fold for $\theta = 0^\circ$. That is, there exists a correlation between changes in the low-frequency and high-frequency peaks. We note that the spectral positions of dip and enhancement correspond to the red and blue side of MM**2** resonance, respectively.

4. Double Fano resonances

4.1. Correlation of double Fano resonances

Now we examine correlation between changes in the low-frequency and high-frequency peaks in terms of double Fano resonances analytically. Let's call the superradiant dipole with low-Q ω_L resonance and the superradiant dipole with high-Q ω_H resonance in DSRR as $u(t)$ and $v(t)$, respectively, and the dipole with ω_M resonance of a rod in FRR as $\zeta(t)$. In the composite metamaterial MM**3**, DSSRs are arrayed with an orientation angle φ. Therefore, upon incidence of a linearly polarized electromagnetic wave with the polarization angle θ, both $u(t)$ and $v(t)$ are excited, and the direction and magnitude of induced dipoles $u(t)$, $v(t)$, and $\zeta(t)$ depend on the angle that the electric field of electromagnetic wave makes with DSRR gap orientation ($\varphi = \frac{\pi}{8}$). Noting that a pair of superradiant dipoles at the upper and lower arcs of DSRR interact with subradiant dipole of FRR symmetrically, dipolar interactions are expressed as

$$U = \Omega_r^2 u(t)\zeta(t)f(\varphi,\theta) + \Omega_r^2 v(t)\zeta(t)g(\varphi,\theta) \tag{3}$$

where $f(\varphi,\theta)$ and $g(\varphi,\theta)$ are the coupling strengths of $u(t)$ and $v(t)$ with $\zeta(t)$, respectively, which are conjugated by the polarization angle θ and the orientation angle φ of DSRR. With external drivings of $u(t)$ and $v(t)$ with $\zeta(t)$ taken into account, the coupled equations of motion are straightforward from Eq. (1) and (2).

$$\frac{d^2u(t)}{dt^2} + \gamma_u\frac{du(t)}{dt} + \omega_u^2 u(t) + \Omega_r^2\zeta(t)f(\varphi,\theta) = \cos(\theta-\varphi)e^{-i\omega_s t} \tag{4}$$

$$\frac{d^2v(t)}{dt^2} + \gamma_v\frac{dv(t)}{dt} + \omega_v^2 v(t) + \Omega_r^2\zeta(t)g(\varphi,\theta) = \sin(\theta+\varphi)e^{-i\omega_s t} \tag{5}$$

$$\frac{d^2\zeta(t)}{dt^2} + \gamma_\zeta\frac{d\zeta(t)}{dt} + \omega_\zeta^2\zeta(t) + \Omega_r^2\{u(t)f(\varphi,\theta) + v(t)g(\varphi,\theta)\} = \eta e^{-i\omega_s t} \tag{6}$$

In the absence of a near-field coupling with the oscillator $\zeta(t)$, two superradiant oscillators $u(t)$ and $v(t)$ are excited independently with the driving amplitudes of $\cos(\theta-\varphi)$ and $\sin(\theta+\varphi)$, respectively. When a near-field coupling with the oscillator $\zeta(t)$ is turned on, there occurs an interplay of $u(t)$ and $v(t)$ through coupling strengths $f(\varphi,\theta)$ and $g(\varphi,\theta)$. The ω_L oscillator $u(t)$ and the ω_H oscillator $v(t)$ reside in one and the same DSRR, and Fano resonances in $u(t)$ and $v(t)$ are correlated. This is similar to the control of EITs in a tripod atomic system where the absorption spectrum of the hyperfine field shows a dependence on the powers of the Zeeman EIT signal [16]. A classical example is to control the absorbed power spectrum of one metal nanoparticle by manipulating the distance between quantum dot and the other metal nanoparticle in a system composed of one quantum dot placed in the gap of two identical metal nanoparticles [17].

An analytical expression of the double Fano resonances by the coupled equations of motion Eq. (4)-(6) allows to identify how the two independent orthogonal superradiant oscillators interact indirectly via a coherent coupling with a common subradiant oscillator.

We compare the spectra of the absorbed power obtained from Eq. (4)-(6) and the measured extinction spectra for polarization angles $\theta = 0^\circ, 45^\circ$, and 90°. In Fig. 5(a), (c), and (e), red and blue curves correspond to the absorbed powers of ω_L and ω_H oscillators of DSRR in MM**1**, and green curve corresponds to the absorbed power of ω_M oscillator of FRR in MM**2**, while gray and pink curves correspond to the absorbed power of ω_L and ω_H oscillators of DSRR in MM**3**, respectively. Black curve is the sum of gray and pink curves. A negative value of the absorbed power by the dipole $v(t)$ in Fig. 5(a) stands for a transfer of power from the dipole $v(t)$ to the dipole $u(t)$, which is observed in Fano resonance in plasmonic structures [27]. We note that the amplitude of dipole $v(t)$ is always positive-definite.

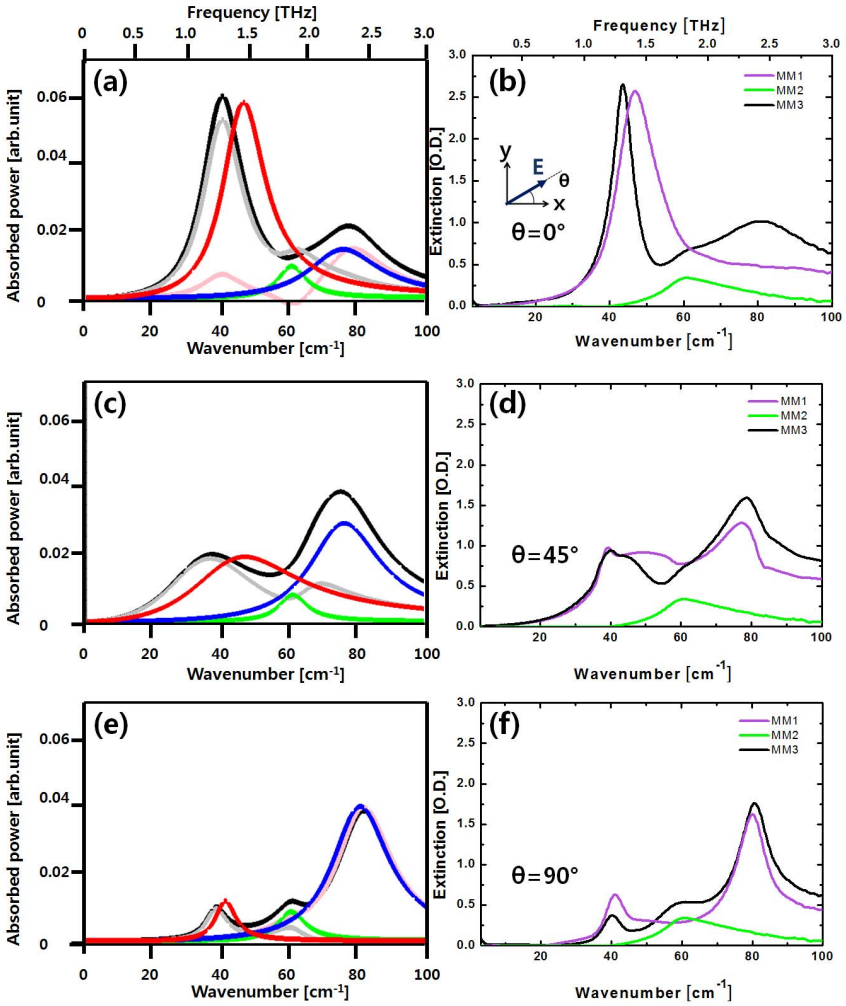

Fig. 5. The spectra (a), (c), and (e) are absorbed powers obtained from the coupled equations. Red, blue, and green curves correspond to the dipoles $u(t)$, $v(t)$, and $\zeta(t)$, respectively. Gray and pink curves brown correspond to the dipoles $u(t)$ and $v(t)$, respectively. Black curve corresponds to the state of DSRR. (b), (d), and (f) are the measured extinction spectra, re-plotted from Fig. 3.

For comparison, in Fig. 5(b), (d), and (f), we plotted black and purple curves corresponding to MM**3** and MM**1**, respectively, along with green curve of MM**2** spectrum. We find that the coupled equations of motion Eq. (4)-(6) describe the relation of MM**3** spectrum and MM**1** & MM**2** spectra appropriately. In other words, in the composite MM**3** possessing tripod plasmonic resonances, the correlation between Fano dip and extinction enhancement stems from an interplay of ω_L and ω_H oscillators in double Fano resonances, mediated by conjugated coupling strengths $f(\varphi,\theta)$ and $g(\varphi,\theta)$ coherently coupled to a common narrow oscillator.

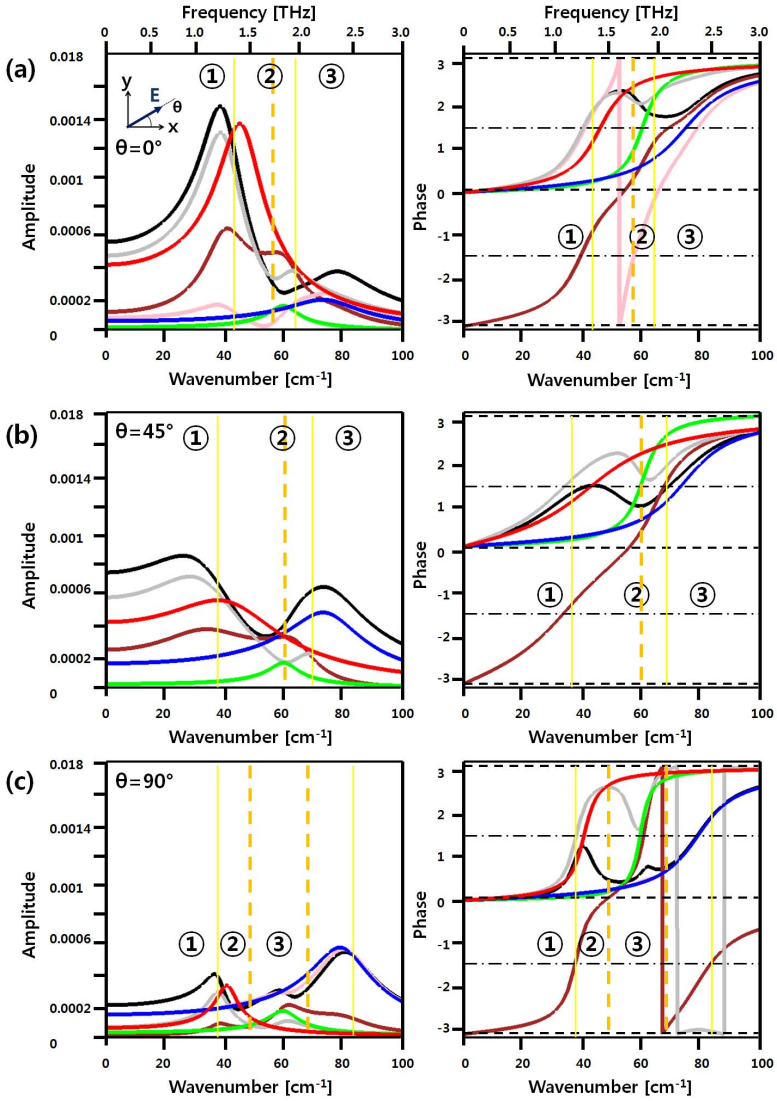

Fig. 6. Amplitude and phase of oscillations of dipoles in MM**3** are shown. Red, blue, and green curves correspond to the dipoles $u(t)$, $v(t)$, and $\zeta(t)$, respectively. Gray, pink, and dark brown curves correspond to the dipoles $u(t)$, $v(t)$, and $\zeta(t)$, respectively. Black curve corresponds to the state of DSRR.

4.2. Phases in double Fano resonances

In a Fano resonance, a destructive interference between superradiant and subradiant modes can be understood by examining how phases of superradiant and subradiant modes evolve upon increasing the driving frequency [33]. In the case that the resonance frequency of subradiant mode is higher than that of superradiant mode, the superradiant mode experiences a phase of $\frac{\pi}{2}$ when going through its own superradiant resonance and the phase keeps on increasing, and when passing through the subradiant resonance the phase experiences a decrease to the minimum phase of a value less than $\frac{\pi}{2}$ and recovers back to its original value, eventually accumulating

to a total value of π. The phase evolution of subradiant mode, however, is very different. The subradiant mode does not experience a decrease in the phase but keeps on accumulating the phase to a total value of 2π by going through superradiant resonance and its own subradiant resonance. Hence near subradiant resonance there occur a spectral region where superradiant and subradiant modes oscillate out-of-phase, which gives rise to a destructive interference for the Fano resonance.

In double Fano resonances taking place in tripod plasmonic resonances, on the other hand, two superradiant modes are coupled to a common subradiant mode, and the phase evolution of one superradiant mode depends on the relative spectral positions of the other superradiant resonance as well as the subradiant resonance. In Fig. 6 are plotted the amplitude and phase of oscillations of 3 dipoles. Red, blue, and green curves correspond to the states of superradiant dipole $u(t)$, superradiant dipole $v(t)$, and subradiant dipole $\zeta(t)$, respectively. Gray, pink, and dark brown curves correspond to the states of superradiant dipole $u(t)$, superradiant dipole $v(t)$, and subradiant dipole $\zeta(t)$, respectively. Black curve corresponds to the state of DSRR containing both superradiant dipoles $u(t)$ and $v(t)$.

Let's examine the the amplitude and phase for the polarization angle $\theta = 0$. As shown in the left panel of Fig. 6(a), three features are distinct from comparison of amplitudes in black with gray and pink curves. In region ① an enhancement of extinction of dipole $u(t)$ takes place owing to the presence of dipole $v(t)$. In region ② two Fano dips (gray and pink curves) in superradiant dipoles $u(t)$ and $v(t)$ are enhanced to one blue-shifted deeper Fano dip (black curve) of DSRR. In region ③ an enhancement of extinction of dipole $v(t)$ takes place owing to the presence of dipole $u(t)$. Phase evolution of DSRR (black curve) in region ② displayed in the center panel Fig. 6(a) shows that the phase recovery of dipole $u(t)$ (gray curve) is hindered by an out-of-phase oscillation of dipole $v(t)$ (pink curve), which explains why Fano dip is enhanced. In regions ① and ③ two dipoles $u(t)$ and $v(t)$ are in-phase, which leads to enhancements of extinction. Enhancement of both extinction and Fano dip is an example of coherent effect in double Fano resonances resulting from coupling of two superradiant oscillators $u(t)$ and $v(t)$ to a common subradiant oscillator $\zeta(t)$ in tripod metamaterial system. In transmission spectrum shown in Fig. 5(b) the coherent effect shows up as an energy transfer from high-Q ω_L oscillator to low-Q ω_H oscillator.

5. Electric field distributions in double Fano resonances

One advantage of the coupled equations of motion Eq. (4)-(6) in describing double Fano resonances is that the coherent oscillation in DSRR containing both $u(t)$ and $v(t)$ can be identified, separately from oscillation in FRR. On the other hand, FDTD provides information on the electric field distribution of MM**3**, which allows us to identify the electric multipolar nature of coherent coupling between DSRR and FRR in MM**3**.

We plot distributions of z-component of electric fields, which are shown in Fig. 7 for $\theta = 0^\circ$. In a planar metamaterial, it is known that z-components of the electric field, normal to the planar metamaterial surface, provide the information on planar charge distributions of the plamonic excitations [34–37]. First of all, we note that excitations in DSRR and FRR of the composite MM**3** are dipolar, similar to dipolar double Fano resonances reported in Ref. [38], where a single dipolar resonance is coupled two dipoles placed side-by-side, and double Fano resonances are observed in opposite ends of the spectrum with respect to a single dipolar resonance. In region ①, dipolar excitation of ω_L oscillator is dominant in DSRR, and the dipoles in DSRR and FRR are anti-parallel forming a bonding hybridization. In region ③, on the other hand, dipolar excitation of ω_S oscillator is dominant in DSRR, and the dipoles in DSRR and FRR are parallel forming an anti-bonding hybridization.

In region ②, Fano dip takes place at the frequency 1.6THz. In order to show explicitly the

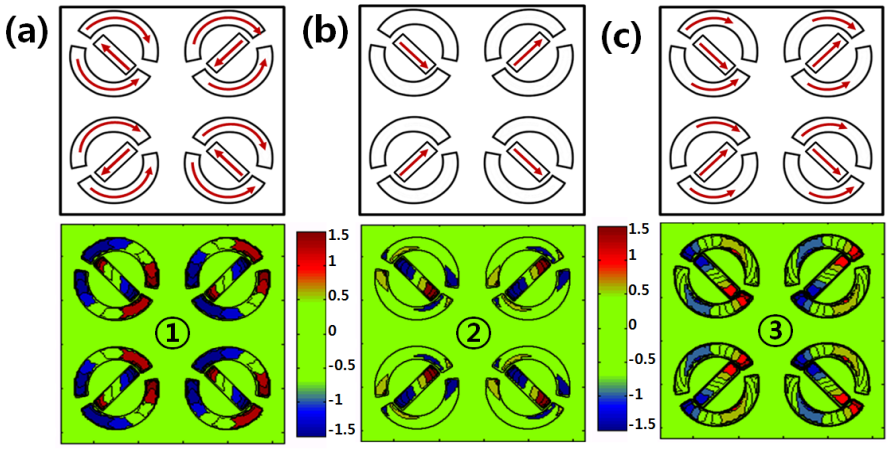

Fig. 7. z-components of near-field electric field, E_z, of MM**3** are plotted for polarization angle $\theta = 0$. (a), (b), and (c) correspond to regions ①, ②, and ③ of Fig. 6, respectively. In particular, (b) corresponds to the frequency 1.8THz which is away from the Fano dip.

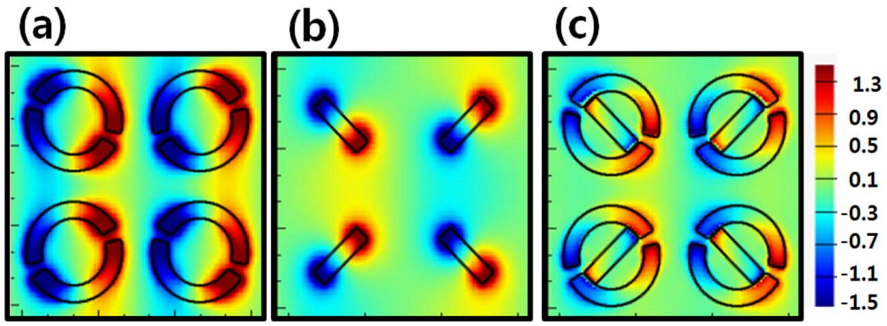

Fig. 8. z-components of near-field electric field, E_z, of (a) the isolated DSRR, (b) the isolated FRR, and (c) the composite MM**3** are plotted at the frequency 1.6THz, where the Fano dip takes place.

excitation of dark mode, distributions of z-component of electric fields in the isolated DSRR, the isolated FRR, and the composite MM**3** are shown in Fig. 8. Comparison of Figs. 8(a) and (c) shows that the induced dipole of DSRR is significantly suppressed by a coherent coupling with FRR, giving rise to the Fano dip in the spectrum of DSRR. Most importantly, the induced dipole of FRR in Fig. 8(c) is opposite to that of FRR in Fig. 8(b).

By comparing dipole-quadrupole and DSRR-FRR Fano resonances, we clarify the Fano mode of dipole excitations in FRR. Figure 9 shows schematics of Fano mode excitations. The left panel represents the uncoupled (a) dipole-quadrupole and (c) DSRR-FRR structures. While a quadrupole is excited in two parallel rods in dipole-quadrupole structure, a weak dipole is excited in FRR MM**2** in DSRR-FRR structure, which is the dipolar excitation observed in Fig. 3. A Fano dip in dipole-quadrupole structure comes from a suppression of dipole excitation owing to a coherent coupling with the quadrupole excitation in two parallel rods as shown in Fig. 9(b). In DSRR-FRR MM**3**, on the other hand, an anti-dipole excitation in subradiant FRR induced by

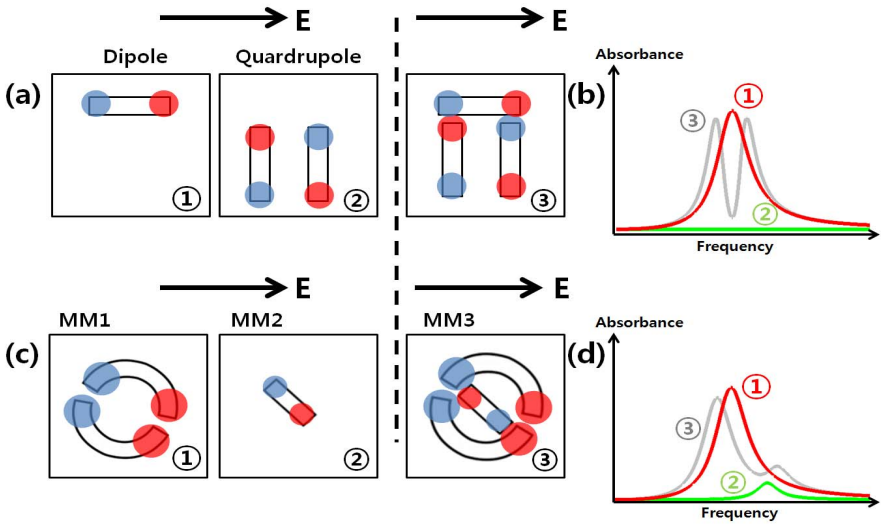

Fig. 9. Schematics of Fano dark mode are drawn for (a) dipole-quadrupole and (b) DSRR-FRR structures at Fano dip.

a near-field coupling with DSRR suppresses a superradiant mode excitation in DSRR of MM**1** as shown in Fig. 9(d).

In other words, the role of anti-dipole in FRR is to polarize DSRR along the direction opposite to the external electric field. There are two pathways for dipole excitations in DSRR. One is a direct dipole excitation along the external electric field direction, and the other is a dipole excitation opposite to the external electric field direction, which originates from the anti-dipole in FRR induced by DSRR. Dipole excitations along these two pathways are coupled coherently leading to a destructive interference, which is exactly the underlying microscopic processes in Fano resonance. In the composite MM**3**, DSRR acts as a superradiant broad oscillator accommodating two resonances of ω_L and ω_H, while dipole in the isotropic FRR corresponds to a subradiant narrow mode.

6. Summary

By embedding four-rod resonators inside double-split ring resonators superlattice, a composite metamaterial system is introduced, where a common subradiant oscillator in four-rod resonator is coupled with two superradiant oscillators in double-split ring resonator to give rise to double Fano resonances. As a classical analogue of four-level tripod atomic system, the transmission spectrum of the composite metamaterial exhibits a double Fano-based coherent effect. Double Fano resonances are correlated owing to the conjugation of two coupling strengths f and g, which shows up as a transfer of absorbed power from one superradiant dipole to the other superradiant dipole in double-split ring resonators. Furthermore, the dipole resonance in FRR is polarization-independent, while two dipole resonances in DSRR are polarization-dependent, which allows for a manipulation of the transfer of absorbed power by the polarization angle of a normally incident electromagnetic wave. Double Fano resonance in a tripod metamaterial system can be utilized in designing plasmonic resonances of metamaterial to engineer coherent effects in metamaterials.

Acknowledgments

We appreciate a reviewer's comment on the original manuscript in bringing up the schematic diagram shown in Fig. 9. This work is supported by the Quantum Metamaterial Research Center program (Ministry of Science, ICT and Future Planning, National Research Foundation, Republic of Korea).